Temperature-Dependent DNA Condensation Triggered by Rearrangement of Adsorbed Cations

Andrey G. Cherstvy,*,†,‡ Alexei A. Kornyshev,†,§,∥ and Sergey Leikin⊥

Institute for Materials and Processes in Energy Systems, Research Center Jülich, D-52425 Jülich, Germany; Institute of Physics, National Academy of Sciences of Belarus, 220072 Minsk, Belarus; Institute for Theoretical Physics II, University of Düsseldorf, D-40225 Düsseldorf, Germany; Department of Chemistry, Faculty of Physical Sciences, Imperial College of Science, Technology and Medicine (University of London), SW7 2AY U.K.; National Institute of Child Health and Human Development, National Institutes of Health, DHHS, Bethesda, Maryland 20892

Received: June 20, 2002; In Final Form: September 18, 2002

A model is suggested explaining observed temperature-favored aggregation of DNA in the presence of Mn^{2+} salts. The interaction between DNA helices is described in terms of screened Coulomb forces and the entropy gain upon DNA aggregation is ascribed to Mn^{2+} repartitioning between binding sites in minor and major grooves. The model rationalizes both the observed force vs separation and entropy vs separation curves provided that the energy and entropy associated with transition of one Mn^{2+} ion from minor to major groove are $\Delta E_{ads} = 3-5\ k_BT$ and $\Delta S_{ads} = 2-5\ k_B$ correspondingly. Although these values appear to be reasonable, no experimental information that would allow their validation is presently available and other interpretations of the observed force curves cannot be excluded.

I. Introduction

Meters of genetic material are packed into the micrometer-size nuclei of living cells. Such compaction is achieved due to condensing effect of specialized biological cations (highly charged histone tails, protamine, spermine, spermidine, etc.). Extensively studied in *in vitro* experiments,[1−12] counterion-induced DNA condensation is also routinely used for DNA purification. Furthermore, DNA condensing ions, e.g., Mn^{2+} are frequently employed in crystallization buffers to obtain X-ray structures of biologically important objects, e.g., nucleosomes.[13] Several theoretical models were proposed to describe different aspects of DNA condensation.[14−21] However, some of the features of this phenomenon are still poorly understood.

One such feature is DNA condensation by Mn^{2+} at elevated temperature. Counterintuitively, temperature-favored aggregation into ordered assemblies is quite common for biopolymers. It was observed not only with Mn−DNA but also with collagen,[22] light chains of myosin,[23] hydroxypropylcellulose,[24] and a number of other macromolecules.[25] Thermodynamic laws dictate that temperature-favored processes must somehow increase the overall entropy of the system. Because formation of an ordered assembly obviously decreases the translational and configurational entropy of macromolecules, there must be some other source of the entropy increase that drives the temperature-favored assembly. Potential sources of entropy increase upon formation of Mn−DNA aggregates are: (i) release of water molecules structured at the DNA surface or in the solvation of Mn^{2+} ions, (ii) reorganization of Mn^{2+} ions bound to DNA,[10] (iii) relaxation (partial melting of DNA backbone) resulting in higher conformational freedom of DNA bases. The question is, which (if any) of these mechanisms is the dominating one?

The release of structured water is a traditional explanation of temperature-favored aggregation of biological macromolecules.[26] It was proposed as the mechanism of temperature effect in Mn^{2+}-induced DNA condensation.[10,27] However, no experimental evidence directly supporting this interpretation was found. Moreover, comparison of strongly temperature-dependent intermolecular forces in Mn−DNA aggregates[10] and temperature-independent, but otherwise similar, forces in cobalt hexammine−DNA aggregates[11] suggests that the temperature dependence may be a peculiar feature of Mn^{2+}, and that other mechanisms should not be overlooked.

Here we consider the potential role of rearrangement of bound Mn^{2+} in the entropy increase observed upon DNA condensation. We base our analysis on the following. It was argued previously that Mn^{2+} as well as some other divalent transition metal ions induce DNA condensation due to their ability to bind in the major groove, particularly to N7 atom of GC base pairs.[28−32] This is in contrast to Ca^{2+} and Mg^{2+} ions, which have much higher binding affinities to DNA phosphates but cannot condense double-stranded DNA. Such ion specificity can be explained by taking into account specific helical symmetry features of the DNA charge pattern.[20,33]

Binding of counterions in the major groove induces a substantial charge separation, resulting in areas of positive and negative charge alternating with 34 Å helical periodicity along the molecular axis. Such charge separation allows alignment of molecules with oppositely charged areas facing each other in a zipper-like fashion, producing an electrostatic attraction sufficiently strong to condense DNA.[20] One expects ions to have much larger translational freedom in the wider major groove compared to ions bound to phosphates in the minor groove. A shift in the equilibrium toward binding in the major groove upon

* Corresponding author: E-mail: a.cherstvy@fz-juelich.de.
† Research Center Jülich.
‡ National Academy of Sciences of Belarus.
§ University of Düsseldorf.
∥ Imperial College.
⊥ National Institutes of Health.

10.1021/jp026343w CCC: $22.00
Published on Web 12/02/2002

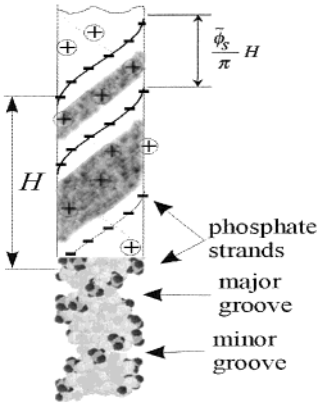

Figure 1. Sketch of B-DNA structure. H is DNA pitch, $\tilde{\phi}_s$ is the azimuthal half-width of the minor groove. Gray bands depict surfaces available for partitioning of adsorbed cations (⊕).

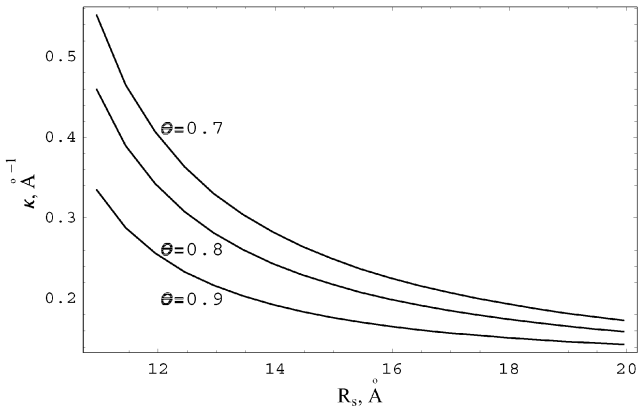

Figure 2. Dependence of the effective κ on the cell radius within the cell model ($a = 9.5$ Å, $n_0 = 0.05$ M, and $T = 20$ °C). The screening length inside the aggregate (κ^{-1}) decreases substantially with increasing aggregate density.

DNA aggregation may, thus, result in a substantial increase in the system entropy and lead to temperature-favored condensation. In the present study we formulate theoretical predictions for this mechanism and compare them with available experimental data. We base our model on the theory of electrostatic interaction between helical macromolecules[33] that accounts for the realistic surface charge pattern of the DNA backbone and distinguishes between different binding sites for counterions.[20,34]

II. Model

DNA Structure and Charge Pattern. Following refs 20, 33, and 34, we assume that bare DNA is a dielectric cylinder with two negatively charged phosphate strands described as spiral line-charges on the cylinder surface (Figure 1). We distinguish two types of counterions: (a) bound, treated as surface charges, and (b) free, treated within the linear Debye−Hückel theory. This two-state model is similar to a Debye−Hückel−Bjerrum approximation in electrolyte theory.[35,36] It may be expected to work reasonably well for Mn−DNA aggregates because most of the counterions providing nonlinear screening of DNA charge are bound within DNA grooves or confined within a very thin layer (~2 Å), smaller than the linear screening length and the distance between surfaces of opposing molecules.

We assume that bound counterions follow the basic double helical motif of DNA. For simplicity, we distinguish only minor and major groove binding and describe the two populations of counterions as positively charged spiral lines located in the middle of the grooves. We calculate the free energy of a hexagonally packed DNA assembly as a function of separation between helices and average occupation numbers for the two types of binding sites (the charge density of the corresponding spiral lines).

This is the simplest model that accounts for the helical symmetry of the surface charge pattern on DNA and possible changes in this pattern upon DNA aggregation. It can be adapted to include other binding sites and generalized to describe each phosphate or counterion as a discrete charge, but this does not change the main qualitative features of intermolecular forces.

Free Energy. Similar to interaction between two DNA helices analyzed previously,[33] it is convenient to represent the free energy per molecule in the DNA hexagonal aggregate in the following form

$$F(R,\theta,f) = F_{cyl}(R,\theta) + F_{helix}(R,\theta,f) + F_{ion}(R,\theta,f) \quad (1)$$

where F is the free energy normalized per unit length of one DNA molecule, R is the interaxial distance between molecules in the aggregate, θ is the fraction of bare DNA charge compensated by bound counterions, and f and $1 - f$ are the fractions of cations in the minor and major grooves correspondingly. The components of the free energy are (i) F_{cyl}, the interaction free energy associated with the average net charge of DNA (free energy of an aggregate of homogeneously charged cylinders whose surface charge density is equal to $(1 - \theta)\bar{\sigma}$, where $\bar{\sigma}$ is the average surface charge density of bare DNA), (ii) F_{helix}, the interaction free energy associated with inhomogeneous, helical pattern of DNA surface charges, and (iii) F_{ion}, the free energy of counterion binding to an isolated DNA molecule.

Homogeneously Charged Cylinders. Calculation of F_{cyl} is a classical problem that was solved with the help of several approximations (see refs 37−39). Because the differences between the results are not substantial and not critical for understanding the temperature sensitivity of Mn−DNA forces, we use the simplest cell model,[38−43] where a molecule is considered to be surrounded by a cylindrical cell of the radius R_s. We calculate the distribution of the electrostatic potential $\Psi(r)$ inside the cell using the Poisson−Boltzmann equation linearized around $\Psi(R_s)$ rather than around the potential in the bulk electrolyte and calculate $\Psi(R_s)$ self-consistently. This leads to renormalized screening length inside the aggregate, κ^{-1} (Figure 2), which reflects the Donnan equilibrium (higher concentration of counterions and shorter screening length compared to that of the bulk electrolyte). We assume that θ is independent of R and of absolute temperature T.

Note that the variation of the potential inside the cell $\Delta\Psi$ does not exceed k_BT/e_0, where e_0 is the elementary charge and k_B is the Boltzmann constant (Figure 3). Consistent with this, detailed comparison shows little difference between our simplified approximation and full numerical solution of the nonlinear Poisson−Boltzmann equation inside the cell. Further details and the expression for F_{cyl} within our model are given in Appendix A. Possible corrections resulting from variation in θ with separation between the molecules are also discussed there.

Helices. We approximate the free energy associated with the helical distribution of charges on DNA by the sum of pair interaction free energies for nearest neighbors derived in ref 20

$$F_{helix}(R,\theta,f) = \frac{48\pi^2\bar{\sigma}^2}{\epsilon\kappa^2}\sum_{n=1}^{\infty}\alpha_n(R)[f\theta + (-1)^n(1-f)\theta - \cos(n\tilde{\phi}_s)]^2 \quad (2)$$

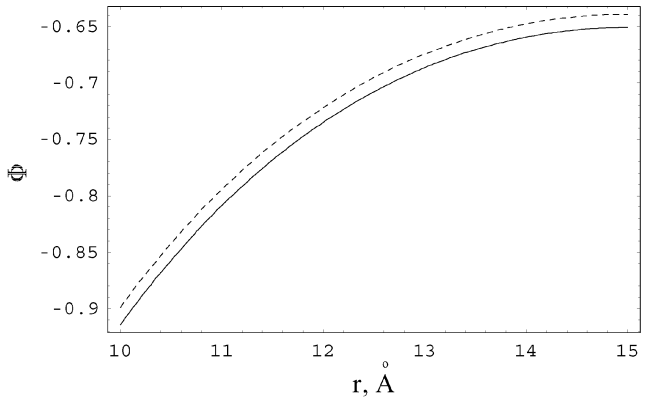

Figure 3. Potential distributions, $\Phi(r) = e_0\Psi(r)/(k_BT)$, in the cell obtained from the linearized solution (solid curve) and the full numerical solution of the nonlinear Poisson−Boltzmann equation (dashed curve) at $n_0 = 0.05$ M (2:1 electrolyte), $\theta = 0.85$, $R_s = 15$ Å, and $T = 20$ °C. The potential drop between the cylinder surface and cell boundary remains small (<1), and the agreement of the two solutions remains reasonably good in the whole range of R_s and temperatures used in the present work.

where ϵ is the macroscopic dielectric constant of water and

$$\alpha_n(R) = \frac{(-1)^n K_0(\kappa_n R) - \sum_{j=-\infty}^{j=+\infty} [K_{j-n}(\kappa_n R)]^2 \dfrac{I_j'(\kappa_n a)}{K_j'(\kappa_n a)}}{[(\kappa_n/\kappa)K_n'(\kappa_n a)]^2} \quad (3)$$

Here $K_n(x)$, $K_n'(x)$ and $I_n(x)$, $I_n'(x)$ are the modified Bessel functions of nth order and their derivatives, $\kappa_n = \sqrt{\kappa^2 + 4\pi^2 n^2/H^2}$, H is the DNA pitch, a is the DNA radius, and $\tilde{\phi}_s$ is the azimuthal half-width of the minor groove (see Figure 1). Following ref 20, we assume that all molecules in the Mn−DNA aggregate are aligned parallel to each other without any axial shifts. Such alignment is energetically favorable at large separations or when a majority of counterions bind in the major groove. For simplicity, we neglect the possibility of other, frustrated alignments (for more detailed analysis of azimuthal alignments of DNA, their frustration and their possible role in various phenomena, see, e.g., refs 44−47). We take into account only the interaction between nearest neighbor molecules because of the rapid, exponential decrease of $\alpha_n(R)$.

Counterion Binding. We neglect short-range interactions between bound cations in the grooves and approximate the free energy of counterion binding by

$$F_{ion}(R,\theta,f) = N_1(E_1 - TS_1) + N_2(E_2 - TS_2) - TS_{conf} \quad (4)$$

Here E_i is the binding energy at a given site in minor ($i = 1$) and major ($i = 2$) grooves. Note that it may have both electrostatic and nonelectrostatic components. S_i is the binding entropy. The axial densities (number per unit length of DNA) of counterions bound in each groove are

$$N_1(R) = \frac{f\theta}{z_+ b} \qquad N_2(R) = \frac{(1-f)\,\theta}{z_+ b} \quad (5)$$

where b^{-1} is the axial density of charged phosphate groups on bare DNA ($b = 1.7$ Å), z_+ is the counterion charge number ($z_+ = 2$ for Mn^{2+}−DNA). Under the assumption that the adsorbed ion is confined between four nearest neighbor phosphates, the linear density of binding sites in each groove is $\bar{N} = 1/(2b)$. To find the configurational entropy of the distribution of bound counterions among these sites, we use a two-state ideal lattice-gas model[48−50] which gives

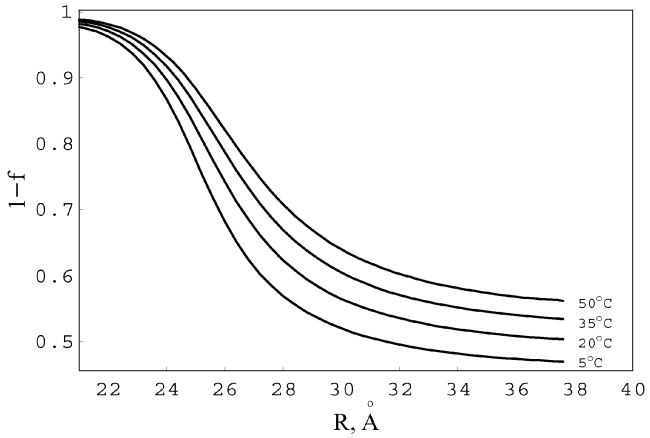

Figure 4. Change in the fraction of cations bound in the major groove, $1 - f$, upon aggregate compression at $n_0 = 0.05$ M, $\theta = 0.85$, $\Delta E_{ads} = 4k_BT$, and $\Delta S_{ads} = 4k_B$. Under these conditions, 4−5 cations per helical pitch of DNA move from the minor to major groove upon aggregate compression.

$$S_{conf}(R) = k_B \sum_{i=1,2} \left[N_i \ln \frac{\bar{N}}{N_i} + (\bar{N} - N_i) \ln \frac{\bar{N}}{\bar{N} - N_i} \right] \quad (6)$$

We assume that $\Delta E_{ads} = E_2 - E_1 > 0$ because of the closer proximity of Mn^{2+} to negatively charged phosphates. We also assume that $\Delta S_{ads} = S_2 - S_1 > 0$, e.g., because of larger space per binding site available in the major groove.

Counterion Partitioning. Equation 1 defines the free energy functional with respect to the minor groove fraction f. Neglecting fluctuations, minimization of eq 1 yields an equation on f

$$f = \frac{1}{2} + \frac{1}{2}\left\{ \frac{(1+K)}{\theta(1-K)} - \sqrt{\left[\frac{(1+K)}{\theta(1-K)} - 1\right]^2 + \frac{4K}{\theta(1-K)}} \right\} \quad (7)$$

Here the partition coefficient K depends on f and R

$$K(f,R) = K(f,\infty) \exp\left\{ -\frac{192\pi^2 b\bar{\sigma}^2}{\epsilon\kappa^2 k_B T} \sum_{n=1}^{\infty} \alpha_n(R)[(-1)^n - 1] \times [f\theta + (-1)^n(1-f)\theta - \cos(n\tilde{\phi}_s)] \right\} \quad (8)$$

and $K(f,\infty) = \exp[-(\Delta E_{ads} - T\Delta S_{ads})/(k_BT)]$.

Intermolecular forces in Mn−DNA aggregates were experimentally studied by the osmotic stress technique,[10,11,51] which directly measures an interaction pressure

$$\Pi(R) = -\frac{dF(R)}{dA} = -\left[\frac{\partial(F_{cyl}(R,\theta) + F_{helix}(R,\theta,f))}{\sqrt{3}R\partial R}\right]_{f,\theta} \equiv p_{cyl}(R,\theta) + p_{helix}(R,\theta,f) \quad (9)$$

where $A = \sqrt{3}R^2/2$ is the cross-section area per molecule in the aggregate. Here we took into account that $\partial F/\partial f = 0$ and $\partial F_{ion}/\partial A = 0$. The two contributions to the interaction pressure are given by

$$p_{cyl} = n_0 k_B T(e^{-2e_0\Psi(R_s,\theta)/k_BT} + 2e^{e_0\Psi(R_s,\theta)/k_BT} - 3) \quad (10)$$

(see Appendix A for derivation), where n_0 is the concentration

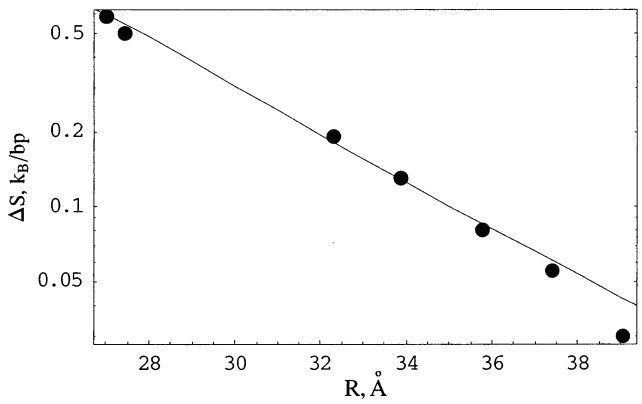

Figure 5. Calculated (solid curve) change in the entropy of adsorbed cations and measured (filled circles, data from ref 27) change in the total entropy upon compression of DNA aggregate at $n_0 = 0.025$ M and $T = 35$ °C. The same θ, ΔE_{ads}, and ΔS_{ads} as in Figure 4 were used for the calculation. Calculated entropy decay length is almost independent on adjustable parameters of the model. The absolute value of ΔS_{ads} has been chosen to get the best agreement with experimental entropy and pressure data.

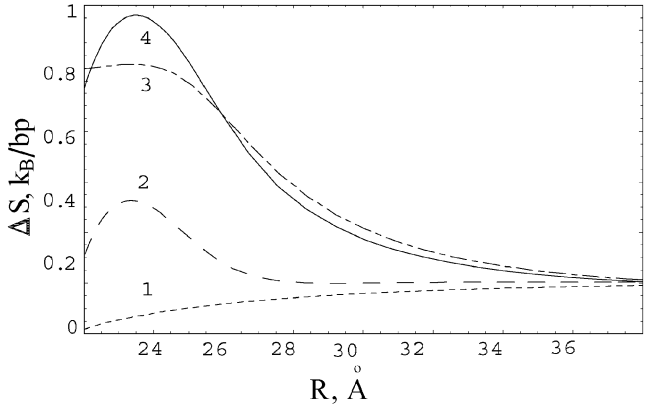

Figure 6. Entropy change with interaxial separation upon DNA aggregate compression. Following eq 1, we distinguish three different contributions to entropy: (1) $S_{cyl} = -\partial F_{cyl}/\partial T$, (2) $S_{helix} = -\partial F_{helix}/\partial T$, and (3) $S_{ion} = -\partial F_{ion}/\partial T$. The total entropy change (4) is dominated by the entropy of repartitioning of ions (S_{ion}). The values of S_{ion} were calculated from eqs 4, 6, and 12. The values of S_{cyl} and S_{helix} were obtained by numerical differentiation of F_{cyl} and F_{helix} where we took into account the measured[52] temperature dependence of water dielectric constant $\epsilon(T)$.

of $MnCl_2$ in the bulk solution outside the DNA aggregate, and according to eq 2[20,33]

$$p_{helix} = \frac{16\sqrt{3}\pi^2\bar{\sigma}^2}{\epsilon R} \times \sum_{n=1}^{\infty} \frac{(-1)^n K_1(\kappa_n R) + 2\sum_{j=-\infty}^{j=+\infty} \frac{K_{j-n}(\kappa_n R) K'_{j-n}(\kappa_n R) I'_j(\kappa_n a)}{K'_j(\kappa_n a)}}{\kappa_n [K'_n(\kappa_n a)]^2} \times [f\theta + (-1)^n(1-f)\theta - \cos(n\tilde{\phi}_s)]^2 \quad (11)$$

Entropy. The model accounts for the following sources of the entropy change with variation of R: (a) the entropy of bound counterions (Figure 5), (b) the entropy of free electrolyte ions and counterions, and (c) the entropy of water polarization fluctuations (at each temperature, we use the observed value of $\epsilon(T)$) (Figure 6). Within this model, the dominating contribution to the entropy change is associated with repartitioning of bound counterions (see Figure 5)

$$\Delta S(R) = \Delta N(R) \Delta S_{ads} + \Delta S_{conf}(R) \quad (12)$$

where $\Delta N(R) = N_2(R) - N_2(\infty)$ is the axial density of cations transferred to the major groove with compression and $\Delta S_{conf}(R) = S_{conf}(R) - S_{conf}(\infty)$; see eq 6.

Model Parameters. The overall entropy change and, thus, the temperature dependence of intermolecular forces depend primarily on ΔS_{ads}. It is the most important adjustable parameter of the model, which, however, cannot be accurately calculated on the basis of present knowledge. Indeed, the value of ΔS_{ads} may depend on the strength of counterion binding in each groove, space available within each binding site, counterion and binding site hydration, etc. It may depend both on the type of counterion and base pair composition of DNA. The two other adjustable parameters, θ and ΔE_{ads}, also depend on some of these factors and may vary upon a change in experimental conditions. The goal of the present work is to see whether the observed force curves and entropy changes can be explained at reasonable values of ΔS_{ads}, θ, and ΔE_{ads}. For the calculations, we use the macroscopic water dielectric constant $\epsilon(T)$[52] and the following values of other parameters: $a \approx 9.5$ Å, $H \approx 34$ Å, $\tilde{\phi}_s \approx 0.4\pi$, and $\bar{\sigma} \approx 16.8$ μC/cm^2.

III. Results and Discussion

Forces and Entropy. Figures 5 and 7 compare the entropy and the osmotic stress vs separation curves measured in columnar aggregates of Mn^{2+}−DNA,[10] and the corresponding curves calculated within our model. The model reproduces experimental observations at reasonable values of the adjustable parameters: $\theta = 0.8-0.9$, $\Delta E_{ads} = 3-5$ k_BT, and $\Delta S_{ads} = 2-5$ k_B. Indeed, $\theta = 0.8-0.9$ agrees with previous estimates for Mn^{2+}−DNA[53] on the basis of the available experimental data. The range of ΔE_{ads} is consistent with our electrostatic estimate of $\Delta E_{ads} \sim 2-8$ k_BT (assuming $\epsilon \sim 20-80$ inside DNA grooves[54]); ΔS_{ads} is expected to be on the order of several k_B. For instance, the geometrically available surface areas per counterion are $A_1 \sim 10$ Å^2 and $A_2 \sim 50$ Å^2 in the minor and major grooves, respectively, so that just the change in the translational entropy upon counterion translocation may already contribute $\sim k_B \ln(A_2/A_1) \sim 1.5k_B$.

Unfortunately, we do not know the contribution of specific (chemical) interactions of bound Mn^{2+} with DNA bases and adjacent phosphates to ΔE_{ads} and ΔS_{ads}. Nor do we know the energetic and entropic cost of the change in solvation of DNA grooves and Mn^{2+} ions upon the ion translocation from the minor to major groove. These unknown factors may change the values (and even the sign) of ΔE_{ads} and ΔS_{ads}. Still, interpretation of the observed data in terms of the described model is plausible.

Within such an interpretation, the net force between DNA helices results from a balance between three main components: (i) repulsion associated with the net, average charge of the molecules, (ii) attraction associated with alignment of negatively charged phosphate strands opposite to positively charged major grooves on adjacent DNA, and (iii) image-charge repulsion of phosphate strands and bound counterions from dielectric cores of adjacent DNA. The average-charge repulsion decreases as $\exp(-\kappa R)$, the attraction decays as $\exp(-\sqrt{\kappa^2+4\pi^2/H^2}R)$, and the image-charge repulsion as $\exp(-2\sqrt{\kappa^2+4\pi^2/H^2}R)$.[33] At larger separations between DNA (prior to the transition to a less hydrated, condensed state) the dominating intermolecular force is the average-charge repulsion.

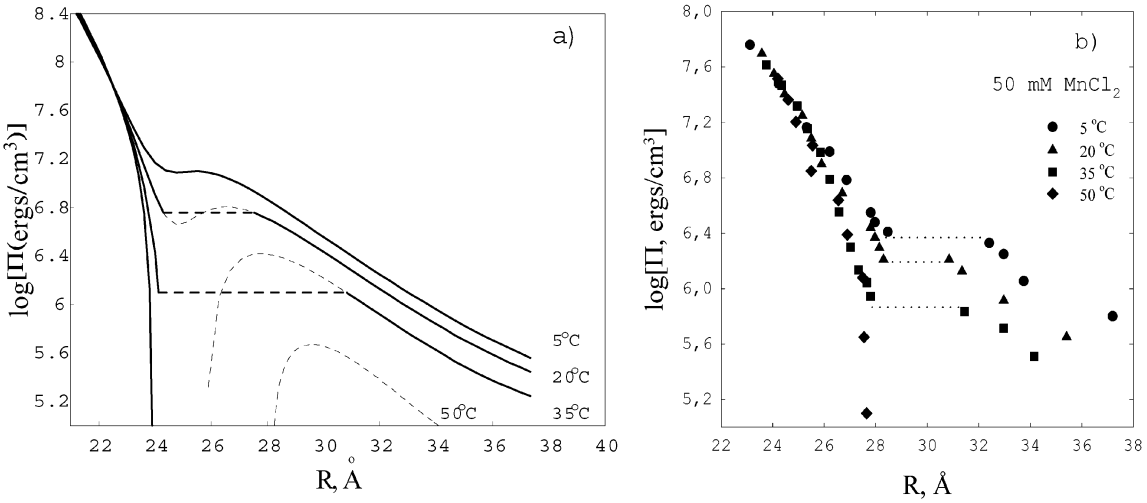

Figure 7. Calculated (a) and measured (b) pressure, Π, in the DNA lattice vs interaxial separation *R* at different temperatures. The same parameters as in Figure 4 were used. The solid lines show the equilibrium pressure−distance curves that exhibit jumpwise transitions from a more hydrated to a less hydrated state. The transitions are indicated by dashed lines. The pressure−distance curve branches that are metastable or unstable at constant pressure (osmotic stress) conditions are depicted by thin dotted curves.

The magnitude of the net force is, however, reduced by the attraction. Elevated temperature favors a higher fraction of counterions in the major groove (due to higher binding entropy). This results in a stronger attraction and smaller absolute value of the net force. At closer distances, the attraction (which increases with decreasing *R* faster than the average-charge repulsion) becomes more important and the net force becomes less repulsive or even attractive. This leads to a jumpwise decrease in the separation under osmotic stress and the transition to the condensed state. In the condensed state, the image-charge repulsion, which has the shortest decay length and the largest amplitude of the three forces, prevents further dehydration. It is responsible for the repulsive branch of the net force observed at close distances.

Counterion Partitioning and Specificity. Because counterion translocation from the minor to major groove increases intermolecular attraction and, thus, reduces the free energy of DNA aggregate, compression of the aggregate by osmotic stress induces such translocation (Figure 4). Most of the counterion repartitioning occurs during the jumpwise transition to the condensed state. Overall, we expect 3−5 bound counterions per helical pitch of DNA (10 base pairs) to move from the minor to major groove with compression. As we have pointed out, the present model associates the observed entropy increase upon DNA condensation and aggregate compression with this repartitioning.

Because it predicts a strong temperature dependence of intermolecular forces only in a fairly narrow range of ΔE_{ads} and ΔS_{ads}, the present model may explain the observed counterion specificity. For instance, assuming that ΔE_{ads} and ΔS_{ads} for Mn^{2+} are within this range, it is natural to expect ΔE_{ads} and ΔS_{ads} for $Co(NH_3)_6^{3+}$ to be substantially different and, therefore, outside the range. Indeed, about 4−5 times lower concentration of $Co(NH_3)_6^{3+}$ was required to induce the same change in the force at room temperature.[10] $Co(NH_3)_6^{3+}$ has a different charge and substantially different size and is capable of forming hydrogen bonds with DNA phosphates. In contrast, preferential binding of Mn^{2+} to guanine N7 in the major groove is believed to be related to interactions involving d-electron orbitals. Because neither Mn^{2+} nor $Co(NH_3)_6^{3+}$ partitioning between DNA grooves is known, we do not know which of these properties has a larger effect on ΔE_{ads} and ΔS_{ads}, but it is reasonable to expect the overall effect to be sufficiently strong to result in very different temperature sensitivity of intermolecular forces in the presence of these ions.

DNA Condensation. Counterion repartitioning, which was analyzed here in the context of osmotic stress experiments, should have a considerable effect on spontaneous DNA condensation induced by corresponding counterions. Our findings shed light on some new aspects possibly important for understanding condensation mechanisms. Indeed, the present model suggests that repartitioning of Mn ions could lead to spontaneous condensation of DNA at elevated temperatures without disruption of the double helix. It also suggests why a similar temperature dependence of DNA condensation was not observed with most other condensing ions, e.g., polyamines and cobalt hexamine. Indeed, the model predicts that a substantial temperature dependence can be observed only within a narrow range of binding energies and entropies. Transition metal ions, including Mn, are believed to bind in DNA grooves because the structure of their electron orbitals leads to favorable interaction with DNA bases. Polyamines and cobalt hexamine are also believed to bind in DNA grooves because of their NH_3 groups, which may form hydrogen bonds with DNA phosphates on both sides of the groove. It is, therefore, natural to expect substantially different binding energies and entropies for the latter ions and, thus, the lack of similar temperature dependence. However, the existing experimental data on DNA condensation do not allow more quantitative comparison with our predictions.

Aggregation-Induced Adsorption of Counterions. We described DNA condensing cations as irreversibly adsorbed in DNA groves, providing a fixed value of θ. We allowed the ions to repartition, but not to leave the surface. If adsorption is not irreversible, θ will increase in response to additional osmotic stress to further neutralize molecules and thus reduce the electrostatic repulsion. The same may happen with spontaneous aggregation. This possibility is discussed in the Appendix in section Adsorption Isotherm. We found that the aggregation-induced adsorption is small. Binding of additional cations during DNA aggregation, possibly more pronounced for $Co(NH_3)_6^{3+}$ [11] than for Mn^{2+},[10] slightly facilitates DNA condensation, but itself it cannot explain the entropy increase upon aggregate compression or the temperature-induced aggregation of Mn^{2+}−DNA assemblies.

Other Interpretations. The interpretation of reported observations in terms of our model is consistent with the available

data. However, the data are not sufficient for excluding other interpretations.

In particular, it was proposed that temperture-induced aggregation of DNA in the presence of Mn^{2+} may be caused by cross-linking of melted sections of DNA mediated by the ions.[55−61] However, Mn^{2+}-induced DNA melting was observed in these works only above 60 °C and at fairly low pH (≃4),[55] i.e., when DNA is substantially less stable than under the conditions of osmotic stress force measurements. Furthermore, such interpretation is at odds with X-ray diffraction patterns observed from Mn^{2+}−DNA aggregates in the latter experiments. Even though it is difficult to exclude that *a fraction* of the sample could be melted, the osmotic stress/X-ray method reveals only the forces between DNA helices that exhibit normal B-DNA scattering pattern and, therefore, have normal double helical structure. Although DNA melting and base pair cross-linking via transition metal ions could be the mechanism of temperature-induced aggregation at low pH and high temperature observed in ref 55, it is unlikely to explain the temperature-dependent forces and aggregation observed at neutral pH and much lower temperatures in refs 10 and 27.

Still, partial destabilization of the DNA backbone by Mn^{2+} may be important even in the latter case. Indeed, aggregation of *nonideally helical* sequences requires torsional deformation of DNA (DNA unwinding from 10.5 bp/turn in solution to 10 bp/turn in the aggregate is observed).[62,63] As previously suggested, this torsional deformation may be needed to make the opposition of negatively charged phosphate strands and positively charged grooves possible over the entire length of the molecules.[64] Otherwise it would be disrupted by sequence-dependent variations in the helical pitch. Partial destabilization of the DNA backbone by Mn^{2+} may reduce torsional rigidity and make the deformation easier. Furthermore, it may increase thermal motions of the backbone. The latter may help to adjust two similar but not completely complementary charge patterns on surfaces of two opposing DNA for a better match. Such temperature-induced complementarity was previously discussed in the context of protein−protein interactions.[65] Although it may give an important contribution to the observed temperature dependence of intermolecular forces between DNA as well, this phenomenon is beyond the scope of the present study and we will analyze it in a separate work.

Finally, here we have rationalized the intermolecular forces in terms of an electrostatic model. Alternatively it was proposed that *hydration forces*, which arise from modulation of the water structure near the DNA surface, may give a substantial contribution to the net interaction.[51,66] It was also argued that the entropy increase associated with the release of structured water upon DNA condensation may be responsible for the observed temperature dependence for Mn^{2+}−DNA.[10] One may speculate that the comparison of the case of Mn^{2+}−DNA which does and $Co(NH_3)_6^{3+}$−DNA which does not exhibit strong temperature dependence suggests that the latter is unlikely related to the release of water structured around sugar−phosphate DNA backbone, because the entropy of such a release should be similar in both cases.

IV. Conclusion

In the present work we focused on the contribution of counterion redistribution on DNA surface to the temperature-induced DNA aggregation. The corresponding model rationalizes the existing observation at reasonable assumptions about the energetic (ΔE_{ads}) and entropic (ΔS_{ads}) costs of this repartitioning. The present work offers a strategy for further experiments. Ideally, one would measure ΔE_{ads} and ΔS_{ads} or partitioning of counterions between DNA grooves and compare the results with our predictions. In reality, direct experiments of this type are difficult to do with existing techniques, but this might be possible in the future.

Although we cannot exclude other interpretations of the studied effects, the predicted electrostatic pressure in DNA assembly is in quantitative agreement with the experimental data. The measured decay length and absolute value of the entropy are also reproduced by our model. All that may be regarded as a strong indication that (i) electrostatic interactions play an important if not dominating role in the behavior of dense ($c_{DNA} \gtrsim 300$ mg/mL) DNA assemblies and (ii) repartitioning of adsorbed Mn^{2+} is likely to be responsible for temperature-induced DNA self-assembly.

Acknowledgment. We are thankful to Per Hansen (NIH), Hartmut Löwen (University of Düsseldorf), Adrian Parsegian (NIH), Don Rau (NIH), and Michael Schurr (University of Washington) for useful discussions. The work was supported by the Deutsche Forschungsgemeinschaft, Grant No. KO 1391/4-1. A.G.C. and A.A.K. thank NICHD, NIH, for the financial support of their visits to Bethesda.

Appendix A: Derivations and Auxiliary Results

Cell Model. The potential in a hexagonal lattice of parallel, homogeneously charged, cylindrical molecules can be approximated by a potential created by molecule inside a cylindrical cell of the radius $R_s = R\sqrt{\sqrt{3}/(2\pi)}$, where R is the DNA−DNA interaxial distance in the lattice.[38,43] Within the standard cell model, the dimensionless electrostatic potential $\Phi(r) = e_0\Psi(r)/(k_BT)$ is described by the nonlinear Poisson−Boltzmann (PB) equation

$$\frac{d^2\Phi(r)}{dr^2} + \frac{1}{r}\frac{d\Phi(r)}{dr} = -4\pi n_0 l_B z_+ (e^{-z_+\Phi(r)} - e^{z_-\Phi(r)}) \quad \text{(A1)}$$

where a is the molecular radius, z_+ and z_- are the valences of electrolyte ions, n_0 is the bulk cation concentration, r is the radial distance from the axis of the cell, $l_B = e_0^2/(\epsilon k_B T)$ is the Bjerrum length, e_0 is the proton charge, k_B is the Boltzmann constant, T is the absolute temperature, and ϵ is the temperature-dependent dielectric constant of water.[52] The following boundary conditions should be satisfied at the molecular surface ($r = a$) and at the cell surface ($r = R_s$)

$$a\left.\frac{\partial\Phi}{\partial r}\right|_{r=a} = 2\xi(1-\theta) \qquad \left.\frac{\partial\Phi}{\partial r}\right|_{r=R_s} = 0 \quad \text{(A2)}$$

where $\xi = l_B/b$, and b is the mean distance between unit negative charges along the axis of the molecule.

Potential Distribution. For the purpose of the present work, we linearize eq A1 near the potential on the cell boundary $\Phi(R_s)$; i.e., we assume that $\Phi(r) = \Phi(R_s) + \delta\Phi(r)$, where $|\delta\Phi(r)| \ll 1$ (see ref 67). Equation A1 then takes the form

$$\frac{d^2\delta\Phi(r)}{dr^2} + \frac{1}{r}\frac{d\delta\Phi(r)}{dr} = -B[-\delta\Phi(r) + A/B] \quad \text{(A3)}$$

where $A = 4\pi l_B n_0 z_+ (e^{-z_+\Phi(R_s)} - e^{z_-\Phi(R_s)})$, $B = 4\pi l_B n_0 z_+ (z_+ e^{-z_+\Phi(R_s)} + z_- e^{z_-\Phi(R_s)})$. This procedure is similar to the so-called Debye−Bjerrum approximation and valid when potential variation inside the cell is small.

The solution of eqs A3 and A2 is

$$\Phi(r,\theta) = \Phi(R_s) + \frac{e^{-z_+\Phi(R_s)} - e^{z_-\Phi(R_s)}}{z_+ e^{-z_+\Phi(R_s)} + z_- e^{z_-\Phi(R_s)}} + \frac{2\xi(1-\theta)}{\kappa a}\frac{I_0(\kappa r)\,K_1(\kappa R_s) + K_0(\kappa r)\,I_1(\kappa R_s)}{I_1(\kappa a)\,K_1(\kappa R_s) - I_1(\kappa R_s)\,K_1(\kappa a)} \quad \text{(A4)}$$

where $\kappa^2 = B = 4\pi l_B n_0 z_+(z_+ e^{-z_+\Phi(R_s)} + z_- e^{z_-\Phi(R_s)})$ is an effective screening length inside the cell. At $r = R_s$, this expression transforms into a transcendental equation that defines the value of $\Phi(R_s)$. Note that the variation of the potential decreases and $\Phi(R_s)$ approaches the Donnan potential with decreasing R_s.

The linearized solution of the PB equation always underestimates the concentration of counterions near a highly charged surface and, therefore, overestimates the surface potential compared to the full solution. However, under the conditions relevant for the present work (strong adsorption of counterions on a molecular surface and substantially reduced net surface charge density), the difference between the linearized solution and full numerical solution of the nonlinear PB equation is small and can be neglected (Figure 3).

Interaction Free Energy and Pressure. Repulsive pressure in the lattice of homogeneously charged cylinders, p_{cyl}, can be expressed via concentrations of ions at the cell boundary ($n_+(R_s)$ and $n_-(R_s)$) and in the bulk ($n_+(\infty)$ and $n_-(\infty)$) as follows[43,68]

$$p_{cyl} = k_B T[n_+(R_s) + n_-(R_s) - n_+(\infty) - n_-(\infty)] = n_0 k_B T\left[e^{-z_+\Phi(R_s)} - 1 + \frac{z_+}{z_-}e^{z_-\Phi(R_s)} - \frac{z_+}{z_-}\right] \quad \text{(A5)}$$

For a 2:1 electrolyte this expression turns into eq 10. A similar expression has been recently used to rationalize the measured osmotic properties of columnar DNA assembly in solutions of simple electrolytes.[37] The free energy of interaction between uniformly charged cylinders can then be found as $F_{cyl}(R) = -\sqrt{3}\int_\infty^R R' p_{cyl}(R')\,dR'$.

Adsorption Isotherm. In the calculations above we assumed that θ is independent of the density of the DNA aggregate. This assumption was based on the experimental observation that the change in the number of adsorbed cations upon compression of Mn−DNA aggregate is ~0.01 per base pair[10] (and, therefore, the change in θ should also be ~0.01, i.e., negligibly small). To test whether such a change is consistent with the parameters used in the present model, we calculated an expected change in θ upon a variation in the cell radius on the basis of a simplified form of the adsorption isotherm,[48,69] which results from equalization of the electrochemical potential of the cations on the molecular surface and in the bulk solution

$$\frac{\theta}{1-\theta} = \frac{n_0}{n_w}\exp\left[-\frac{F_{ads}}{k_B T}\right]\exp[-z_+\Phi(a,\theta)] \quad \text{(A6)}$$

where $n_w = 55.5$ M is the water molarity, F_{ads} is the adsorption free energy, and $\Phi(a,\theta)$ is the surface potential in the cell model.

The dependence of θ on R_s calculated from eqs A6 and A4 at different values of F_{ads} is plotted in Figure 8. We find that the change in θ is indeed ~0.01 when $\theta(\infty)$ exceeds 0.8−0.85, which is the range of θ required for Mn^{2+}-induced condensation within our model and in experiments.[10] Note that for high DNA charge neutralization the effect of $\theta(R_s)$ dependence in this model of adsorption has, practically, no effect on the pressure isotherm at large interaxial separation ($R \gtrsim 35$ Å). At small separation ($R \lesssim 23$ Å), where the image-charge-repulsion dominates, this effect is only slightly pronounced. The value of the adsorption free energy that produces such θ ($F_{ads} \sim 10\ k_B T$) has the same order of magnitude but is slightly larger than the change in the adsorption free energy upon Mn^{2+} transition from the minor to major groove. In other words, it also appears to be consistent with model assumptions required for explaining the observed temperature dependence.

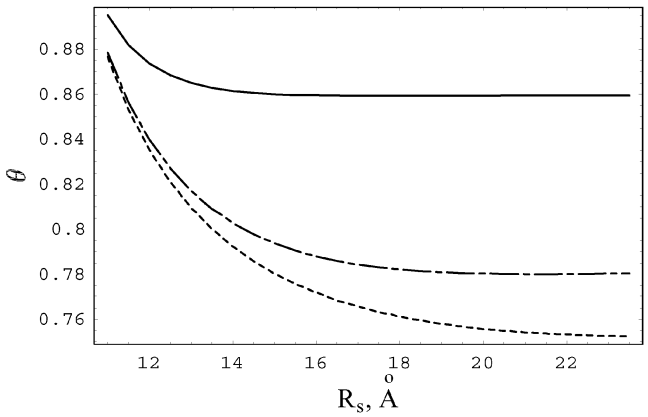

Figure 8. Dependence of DNA charge compensation θ on a molecule in the cell on the adsorption free energy according to (A6). Parameters: $n_0 = 0.05$ M, $F_{ads}/(k_B T) = -3$ (dotted), -6 (dotted-dashed), -9 (solid) curves. θ increases with compression because the value of surface potential increases. The larger the value of θ, the smaller its variation with compression.

References and Notes

(1) Bloomfield, V. A.; Wilson, R. W.; Rau, D. C. *Biophys. Chem.* **1980,** *11*, 339.
(2) Wilson, R. W.; Bloomfield, V. A. *Biochemistry* **1979,** *18*, 2192.
(3) Ma, C.; Bloomfield, V. A. *Biopolymers* **1995,** *35*, 211.
(4) Ma, C.; Bloomfield, V. A. *Biophys. J.* **1994,** *67*, 1678 and references therein.
(5) Widom, J.; Baldwin, R. L. *J. Mol. Biol.* **1980**, *144*, 431.
(6) Bloomfield, V. A. *Biopolymers* **1991**, *31*, 1471.
(7) Bloomfield, V. A. *Biopolymers* **1997**, *44*, 269.
(8) Pelta, J.; Livolant, F.; Sikorav, J.-L. *J. Biol. Chem.* **1996**, *271*, 5656.
(9) Pelta, J.; Durand, D.; Doucet, J.; Livolant, F. *Biophys. J.* **1996**, *71*, 48.
(10) Rau, D. C.; Parsegian, V. A. *Biophys. J.* **1992**, *61*, 260.
(11) Rau, D. C.; Parsegian, V. A. *Biophys. J.* **1992**, *61*, 246.
(12) Rau, D. C.; Lee, B.; Parsegian, V. A. *Proc. Natl. Acad. Sci. U.S.A.* **1984**, *81*, 2621.
(13) Luger, K.; Mäder, A. M.; Richmond, R. K.; Sangent, D. F.; Richmond, T. J. *Nature* **1997,** *389*, 251.
(14) Podgornik, R.; Parsegian, V. A. *Phys. Rev. Lett.* **1998**, *80*, 1560.
(15) McFail-Isom, L.; Sines, C. C.; Williams, L. D. *Curr. Opin. Struct. Biol.* **1999**, *9*, 298.
(16) Ha, B.-Y.; Liu, A. J. *Phys. Rev. E* **1999**, *60*, 803.
(17) Ha, B.-Y.; Liu, A. J. *Phys. Rev. Lett.* **1998**, *81*, 1011 and references therein.
(18) Shklovskii, B. I. *Phys. Rev. Lett.* **1999** , *82*, 3268.
(19) Widom, J.; Baldmin, R. L. *Biopolymers* **1983**, *22*, 1595.
(20) Kornyshev, A. A.; Leikin, S. *Phys. Rev. Lett.* **1999**, *82*, 4138.
(21) Lyubartsev, A. P.; Nordenskiöld, L. *J. Phys. Chem.* **1995**, *99*, 10373.
(22) Leikin, S.; Rau, D. C.; Parsegian, V. A. *Proc. Natl. Acad. Sci. U.S.A.* **1994**, *91*, 276.
(23) Gill, T. A.; Chan, J. K.; Prochareon, K. F.; Paulson, A. T. *Food Res. Int.* **1992**, *25*, 333.
(24) Bonnet-Gonnet, C.; Leikin, S.; Chi, S.; Rau, D. C.; Parsegian, V. A. *J. Phys. Chem. B* **2001**, *105*, 1877.
(25) Rau, D. C.; Parsegian, V. A. *Science* **1990**, *249*, 1278.
(26) Lauffer, M. A. *Entropy-driven processes in biology*; Springer: Berlin, 1975.
(27) Leikin, S.; Rau, D. C.; Parsegian, V. A. *Phys. Rev. A* **1991**, *44*, 5272.
(28) Eichhorn, G. L.; Shin, Y. Ae. *J. Am. Chem. Soc.* **1968**, *90*, 7323.
(29) van Steenwinkel, R.; Campagnari, F.; Merlini, M. *Biopolymers* **1981**, *20*, 915.
(30) Clement, R. M.; Sturm, J.; Daune, M. P. *Biopolymers* **1981**, *21*, 405.
(31) Granot, J.; Kearns, D. R. *Biopolymers* **1982,** *21*, 203, 219, 873.

(32) Saenger, W. *Principles of nucleic acid structure*; Springer-Verlag: New York, 1984.
(33) Kornyshev, A. A.; Leikin, S. *J. Chem. Phys.* **1997**, *107*, 3656; Erratum. *J. Chem. Phys.* **1998**, *108*, 7035(E).
(34) Kornyshev, A. A.; Leikin, S. *Proc. Natl. Acad. Sci. U.S.A.* **1998**, *95*, 13579.
(35) Fisher, M. E.; Levin, Y. *Phys. Rev. Lett.* **1993**, *71*, 3826.
(36) Zuckerman, D. M.; Fisher, M. E.; Lee, B. P. *Phys. Rev. E* **1997**, *56*, 6569.
(37) Hansen, P. L.; Podgornik, R.; Parsegian, V. A. *Phys. Rev. E* **2001**, *64*, 0219071.
(38) Fuoss, R. M.; Katchalsky, A.; Lifson, S. *Proc. Natl. Acad. Sci. U.S.A.* **1951**, *37*, 579.
(39) Katchalsky, A.; Lifson, S. *J. Polym. Sci.* **1954**, *XIII*, 43.
(40) Alfrey, T.; Berg, P. W.; Morawetz, H. *J. Polym. Sci.* **1951**, *VII*, 543.
(41) Rice, S. A.; Nasagawa, M.; Morawetz, H. *Polyelectrolyte Solutions*; Academic Press: London, New York, 1961.
(42) Frank-Kamenetskii, M. D.; Anshelevich, V. V.; Lukashin, A. V. *Sov. Phys. Usp.* **1987**, *30* (4), 317.
(43) Katchalsky, A. *Pure Appl. Chem.* **1971**, *26*, 327.
(44) Langridge, R.; Wilson, H. R.; Hooper, C. W.; Wilkins, F.; Hamilton, L. D. *J. Mol. Biol.* **1960**, *2*, 19.
(45) Strey, H. H.; Wang, J.; Podgornik, R.; Rupprecht, A.; Yu, L.; Parsegian, V. A.; Sirota, E. B. *Phys. Rev. Lett.* **2000**, *84*, 3105−3108.
(46) Podgornik, R.; Strey, H. H.; Gawrisch, K.; Rau, D. C.; Rupprecht, A.; Parsegian, V. A. Proc. *Natl. Acad. Sci. U.S.A.* **1996**, *93*, 4261.
(47) Harreis, H. M.; Kornyshev, A. A.; Likos, C. N.; Löwen, H.; Sutmann, G.; *Phys. Rev. Lett.* **2002**, *89*, 018303−1.
(48) Adamson, A. W.; Gast, A. P. *Physical Chemistry of Surfaces*, 6th ed.; Wiley-Interscience Publication: New York, 1997.
(49) Gurevich, Yu. Ya.; Kharkats, Yu. I. *Sov. Phys. Dokl.* **1976**, *21*, 642.
(50) Kornyshev, A. A.; Vorotyntsev, M. A. *Electrochim. Acta* **1981**, *26*, 303.
(51) Leikin, S.; Rand, R. P.; Rau, D. C.; Parsegian, V. A. *Annu. Rev. Phys. Chem.* **1993**, *44*, 369.
(52) *CRC Handbook of Chemistry and Physics*, 75th ed.; Lide D. R., Ed.; CRC Press: Boca Raton, FL, 1994.
(53) Rau, D. C. Unpublished results.
(54) Lamm, G.; Pack, G. R. *J. Phys. Chem.* **1997**, *101*, 959.
(55) Duguid, J. G.; Bloomfield, V. A.; Benevides, J. M.; Thomas, G. J., Jr. *Biophys. J.* **1995**, *69*, 2623.
(56) Duguid, J. G.; Benevides, J. M.; Bloomfield, V. A.; Thomas, G. J., Jr. *Biophys. J.* **1993**, *65*, 1916.
(57) Duguid, J. G.; Bloomfield, V. A. *Biophys. J.* **1995**, *69*, 2642.
(58) Yurgaitis, A. P.; Lasurkin, Yu. S. *Biopolymers* **1981**, *20*, 967.
(59) Knoll, D. A.; Fried, M. G.; Bloomfield, V. A. In *Structure and Expression: DNA and its drug complexes*; Sarma, M. H., Sarma, R. H., Eds.; Adenine Press: New York, 1988; Vol. 2, p 123.
(60) Matulis, D.; Rouzina, J.; Bloomfield, V. A. *J. Mol. Biol.* **2000**, *296*, 1053.
(61) Shibata, J. H.; Schurr, J. M. *Biopolymers* **1981**, *20*, 525.
(62) Rhodes, D.; Klug, A. *Nature* **1981**, *292*, 378.
(63) Zimmerman, S. B.; Pheiffer, B. H. *Proc. Natl. Acad. Sci. U.S.A.* **1979**, *76*, 2703.
(64) Kornyshev, A. A.; Leikin, S. *Phys. Rev. Lett.* **2001**, *86*, 3666.
(65) Leikin, S.; Parsegian, V. A. *Proteins* **1994**, *19*, 73.
(66) Leikin, S. In *Hydration processes in biology: theoretical and experimental approaches*; Belissent-Funel, M.-C., Eds.; IOS Press: Amsterdam, 1999; p 313, 323.
(67) Lifson, S. *J. Chem. Phys.* **1957**, *27*, 700.
(68) Verwey, E. J. W.; Overbeek, J. Th. G. *Theory of the stability of lyophobic colloids*; Elsevier Press: Amsterdam, The Netherlands, 1948.
(69) Lyklema, J. In *Adsorption from solution at the solid/liquid interface*, Parfitt, G. D., Rochester, C. H., Eds.; Academic Press: 1983; p 239.